J Mater Sci (2011) 46:1341–1350
DOI 10.1007/s10853-010-4925-2

# Organic solvent based $TiO_2$ dispersion paste for dye-sensitized solar cells prepared by industrial production level procedure

**Ryohei Mori · Tsutomu Ueta · Kazuo Sakai · Yasuhiro Niida · Yasuko Koshiba · Li Lei · Katsuhiko Nakamae · Yasukiyo Ueda**

Received: 7 May 2010 / Accepted: 13 September 2010 / Published online: 28 September 2010
© Springer Science+Business Media, LLC 2010

**Abstract** In order to prepare the $TiO_2$ liquid dispersions for the electrodes of dye-sensitized solar cells with industrial mass production level at a reasonable cost, the present study investigates the preparation of $TiO_2$ liquid dispersions by a general industrial dispersion technique using readily available P25. To determine the $TiO_2$ dispersion offering the best light–electricity energy conversion efficiency, the suitability of various types of solvents and resins for use in $TiO_2$ dispersion are tested. In general, organic solvent based $TiO_2$ dispersions are found to allow the formation of more uniform thin films in comparison with water-based dispersions. A preparation using ethyl cellulose as the resin and the terpineol as the solvent is found to exhibit the best conversion efficiency. We have also found that using two kinds of resins of different molecular weights gave rise to better efficiency. Among 26 metal compounds tested in this study, the best metal dopant was Ag. XRD and XPS measurements confirm that the Ag exists as metal Ag and silver oxide.

## Introduction

Regenerative dye-sensitized photoelectrochemical cells have been under investigation for the past decades. The low production costs, together with a good efficiency of energy conversion, reaching 10% in some cases, make such devices a promising alternative for the development of a new generation of solar cells [1–4]. In order to achieve high cell energy efficiency, much previous research has been directed toward improving the photocurrent and photovoltage by, for example, developing new sensitizers [5–8], increasing the light-scattering properties of the film [9, 10], suppressing the charge recombination [2, 11, 12], improving the interfacial energetic mechanism [13, 14], and altering the particle morphology [3, 15–17]. However, the efficiency values obtained through these approaches thus far are still less than half the theoretical value, and are not large enough for practical use [18]. Against this background, the inclusion of metal ion doping offers a practical way of providing additive properties such as visible light response to a $TiO_2$ film, since $TiO_2$ is active only under ultraviolet light due to its wide band gap ($\sim$3.0 eV) [19–21].

However, there is as yet insufficient fundamental research considering the application to practical industrial use at reasonable costs. For example, T/SP $TiO_2$ paste (Solaronix SA, Switzerland) is currently prepared by a hydrothermal method, but this method is too expensive for industrial use. However, the much cheaper alternative approach of manufacturing a $TiO_2$ liquid dispersion by a general dispersion technique using bead mill machines potentially presents an ideal procedure for the mass production of $TiO_2$ electrode film.

In this study, we have focused on preparing a $TiO_2$ liquid dispersion with readily available P25 using a general dispersion technique, and attempted to find the best solvent and resin combination, including a consideration of water-based system, as well as the best metal dopant to enhance the light-to-electricity conversion efficiency.

R. Mori (✉) · T. Ueta · K. Sakai
Fuji Pigment Co., Ltd, Kawanishi, Japan
e-mail: moriryohei@fuji-pigment.co.jp

Y. Niida · Y. Koshiba · Y. Ueda
Graduate School of Science and Technology, Kobe University, Kobe, Japan

L. Lei · K. Nakamae
Hyogo Science and Technology Association, Ako, Japan

## Experimental

A range of $TiO_2$ liquid dispersions were prepared by mixing P25 (Nippon Aerosil Co. Ltd, Japan) with various types of organic solvent and water, while resin was also used as a binder. Polyoxyethylene sorbitane mono laurate (Kao Corporation Co. Ltd, Japan) was used as dispersant for the water-based mixtures, whereas alkylolammonium salt of a block copolymer with an acidic group (BYK-Chemie GmbH, Germany), was used as the dispersant for the organic solvent based mixtures. A $TiO_2$ sol slurry was prepared with P25 according to the following procedure. Using a paint shaker (Red Devil Equipment Co., USA), P25 was dispersed in water or an organic solvent. Paint shaker can mix pigment, solvent, dispersant, various type of additives etc., in plastic bottle with ceramic beads inside, by simply shaking intensively for a certain period of time. Various types of resin, such as polyethylene glycol (PEG, Dai-ichi Kogyo Seiyaku, Co. Ltd, Japan, MW 20000) or ethyl cellulose (Dow Chemical Inc. USA), were then added to act as a binder and also to increase the viscosity of the $TiO_2$ dispersion for use in the squige printing technique, and to allow the preparation of a porous thin film after sintering. For example, to prepare sample 3 in Table 1, 21 g of P25, 3 g of dispersant, and 46 g of terpineol (Arakawa Chemical Industries, Co.Ltd, Japan) were added in a plastic bottle, then mixed with paint shaker. Please note that 100 mL of ceramic (zirconia 0.6–0.8 mm) beads should be added in order to disperse and mix the content inside of the plastic bottle. Then, an appropriate amount of ethyl cellulose was added to obtain the final $TiO_2$ paste for the electrode. The quantity of added ethyl cellulose was 9.0% for the sample (3, 4, 5 8, 11), whereas it was 6.4% (MW 60,000) and 1.8% (MW 110,000) for the sample (1, 2, 6, 7, 9, 10) in Table 2.

Metal doping was carried out by adding metal compounds in chloride, nitrate, alkoxide, and other metal forms, into the $TiO_2$ dispersion. In this study, a $TiO_2$ dispersion with doped metal content in molar ratio Ti:metal = 100:X will be referred to as a metal-X $TiO_2$ film. For example, $TiO_2$ film with doped Ag content in molar ratio Ti:Ag = 100:1 is referred to as an Ag-1 $TiO_2$ film. For Nb and Ag doping, niobium ethoxide and silver nitrate (for both, Wako Pure Chemical Industries, Ltd, Japan) were, respectively, used in this study.

For morphology observation, the resultant $TiO_2$ viscous paste was deposited on ITO coated glass (Nippon Sheet Glass Co., Ltd, Japan) by the squige printing technique followed by heating at 450 °C for 30 min, and then allowed to cool down to room temperature. An atomic force microscope (SPI 3800 N, Seiko Instruments Co. Ltd, Japan) and a transmission electron microscopy (TEM, Hitachi, H-7100) were used. Thermogravimetry (TG) and differential thermal analysis (DTA) were performed using a TG-DTA system (Thermoflex TG 8110, Rigaku Co. Ltd, Japan) to evaluate the thermal properties of the titania gel. This dried gel was prepared just simply by leaving the titania paste at ambient atmosphere over 2 months.

For $TiO_2$ particle size measurement, titania paste was diluted into solvent 200 times, then the size of $TiO_2$ particle in liquid was analyzed using particle size characterization (Microtrac, UPA-EX 150, Nikkiso Co.Ltd, Japan). The crystal phase of the $TiO_2$ was evaluated by X-ray diffractometry (XRD, Rigaku, RINT1200 X-ray diffractometer)

**Table 1** Photovoltaic characteristics of dye-sensitized solar cells prepared from $TiO_2$ dispersion paste with various type of solvent and resin combination prepared in this study

| Sample | Resin | Solvent | Film formation | $TiO_2$ (P25) content (%) | $J_{sc}$, short circuit current (mA/cm$^{-2}$) | $V_{oc}$, open circuit voltage (mV) | FF, fill factor | $\eta$, energy conversion efficiency |
|---|---|---|---|---|---|---|---|---|
| 1 | Poly vinyl butyral | Terpineol | ○ | 27.4 | 10.79 | 717 | 0.568 | 4.40 |
| 2 | Ethyl cellulose | Diethylene glycol, mono methyl ether | ○ | 24.8 | 10.93 | 710 | 0.528 | 4.10 |
| 3 | Ethyl cellulose | Terpineol | ○ | 24.8 | 13.03 | 708 | 0.496 | 4.57 |
| 4 | Aclylic polymer | Terpineol | × | 24.8 | | | | |
| 5 | Cellulose acetate buttylate | Diethylene glycol, mono methyl ether | ○ | 25.7 | 11.57 | 703 | 0.532 | 4.32 |
| 6 | PEG | Water | ○ | 18.8 | 8.21 | 713 | 0.480 | 2.81 |
| 7 | Hydroxy propyl cellulose | Water | × | 18.8 | | | | |
| 8 | Xanthan gum | Water | × | 18.8 | | | | |
| 9 | Methyl cellulose | Water | × | 18.8 | | | | |
| 10 | Poly vinyl alcohol | Water | × | 18.8 | | | | |
| 11 | Poly vinyl pyrrolidone | Water | × | 18.8 | | | | |

○ without cracking, × cracked film

**Table 2** Photovoltaic characteristics of dye-sensitized solar cells prepared from $TiO_2$ dispersion paste (ethyl cellulose as resin, terpineol as solvent) with various type of molecular weight, dispersing time, size of the bead used in this study

| Sample | Resin (MW) | Dispersing time (min) | Beads diameter | $TiO_2$ (P25) content (%) | $J_{sc}$, short circuit current (mA/cm$^{-2}$) | $V_{oc}$, open circuit voltage (mV) | FF, fill factor | $\eta$, energy conversion efficiency |
|---|---|---|---|---|---|---|---|---|
| 1 | 60,000 + 110,000 | | | 24.8 | 12.88 | 709 | 0.489 | 4.47 |
| 2 | 60,000 + 110,000 | | | 27.4 | 13.03 | 708 | 0.496 | 4.57 |
| 3 | 90,000 | 15 | 0.6–0.8 mm zircon | 24.8 | 11.32 | 729 | 0.507 | 4.18 |
| 4 | 40,000 | | | 24.8 | 8.62 | 688 | 0.521 | 3.09 |
| 5 | 200,000 | | | 24.8 | 9.62 | 681 | 0.533 | 3.49 |
| 6 | 60,000 + 110,000 | | | 24.8 | 7.60 | 671 | 0.576 | 2.94 |
| 7 | 60,000 + 110,000 | 60 | 0.6–0.8 mm zircon | 24.8 | 6.31 | 677 | 0.565 | 2.41 |
| 8 | 90,000 | | | 24.8 | 7.12 | 680 | 0.572 | 2.77 |
| 9 | 60,000 + 110,000 | | | 24.8 | 6.21 | 640 | 0.540 | 2.14 |
| 10 | 60,000 + 110,000 | 120 | 0.3 mm zirconia | 24.8 | 7.95 | 647 | 0.528 | 2.72 |
| 11 | 90,000 | | | 24.8 | 7.34 | 662 | 0.539 | 2.62 |

using Cu $K_\alpha$ radiation operated at 40 kV and 40 mA, and the first crystallite size of $TiO_2$ was calculated from a half-value width of the XRD peak at $2\theta = 25.4°$ using Scherrer's equation. The molar ratio of doped metal in $TiO_2$ was measured by X-ray photoelectron spectroscopy (XPS, Ulvac-phi 5500 MT X-ray photoelectron spectrometer). The binding energy was calibrated by a thin gold film vacuum-deposited on the sample. The spectra were decomposed into Gaussian functions with a computer program supplied by Ulvac-Phi. The BET surface area was determined by a surface area analyzer (Shimadzu, Aquasorb 2100E). Sample was prepared by heating 10 g of $TiO_2$ paste at 450 °C for 30 min, and then allowed to cool down to room temperature as we have treated when we prepared $TiO_2$ film electrode. The pore size distribution was also determined by the BJH method of nitrogen desorption measurements (Shimadzu, Autopore IV9510).

For solar cell characterization, $TiO_2$/ITO films were immersed in a $3 \times 10^{-3}$ M ruthenium complex dye (N-719) (ruthenium (2,2′-bipyridyl-4,4′-dicarboxylate)$_2$ (NCS)$_2$) in a mixture of ethanol and *tert*-butanol (50/50 v/v) solution at room temperature for 15 h in the dark. $TiO_2$ electrode was rinsed with acetonitrile and dried. Then, the amount of adsorbed dye was determined by dissolving the dye from the $TiO_2$ surface into a 0.1 M NaOH aqueous solution, and measuring its absorbance by a UV–visible light spectrometer.

The electrolyte solution was composed of 0.1 M of lithium iodide, 0.05 M of iodine, 0.5 M of *tert*-butylpyridine, and 0.6 M of 2,3-dimethyl-1-propylimidazolium iodide in acetonitrile.

The photovoltaic properties of the $TiO_2$/dye/$I^-$, $I_3^-$/Pt cells were estimated by recording the current–voltage characteristics of each cell (MP-160, Eko Instruments Co., Ltd) under an illumination of AMl.5 (100 mW cm$^{-2}$) using a solar simulator. The spectrum of simulated solar light was calibrated against the JIS amorphous-Si Standard. The area of the dye-coated $TiO_2$ electrode was 0.28 cm$^2$.

## Results and discussions

### Influence of resin and solvent

Table 1 summarizes the photovoltaic characteristics of $TiO_2$ thin films prepared from various types of resins and solvents. It can be seen that the film prepared using ethyl cellulose as the resin, and terpineol as the solvent, has exhibited the highest light-to-electricity energy conversion efficiency. When water was used as the solvent, only PEG exhibited a stable film formation on transparent conductive glass. It was found to be impossible to create uniform $TiO_2$ films using other water-soluble resins listed in Table 1 (hydroxy propyl cellulose, xanthan gum, methyl cellulose, etc…). They exhibited a cracked surface that was recognized by naked eye observation, and gave no photocurrent under light illumination. On the other hand, when an organic solvent was used as solvent, most of the $TiO_2$ dispersions enabled us to form uniform thin films. One can say that the organic solvent based $TiO_2$ dispersions seem to offer the most promising approach for industrial mass level use. It should be noted here that all of the $TiO_2$ thin films prepared in this study possess film thickness ranging from 7.5–9.0 μm.

Table 2 summarizes the influences of the molecular weight of resin and its concentration, the dispersion time, and bead diameter, on energy conversion efficiency. In Table 2, all of the samples are made from $TiO_2$

dispersion in which the ethyl cellulose was used as resin, and the terpineol as solvent. Energy conversion efficiency was relatively higher when two kinds of ethyl cellulose with different molecular weights were used. It was quite obvious that conversion efficiency was lower when the smallest (MW 44,000) and largest (MW 200,000) ethyl cellulose was applied to prepare the $TiO_2$ dispersion. This means there is an optimum resin molecular size for $TiO_2$ film electrode. The detail research is remained to investigate the influence caused by the size of the resin. Here, MW indicates mass average MW.

Dispersion time was found to be also critical. Conversion efficiency decreased when dispersing time was more than 1 h. When we use a "paint shaker" or "bead mill" machine for liquid dispersion preparation, generally beads of smaller diameter give rise to smaller nanoparticles as long as the beads are made of the same material. In the present case either zircon or zirnonia. In our study, efficiency decreases when smaller beads and a longer dispersion time were applied (0.3 mm zirconia, 120 min). It is deduced that when $TiO_2$ nanoparticles size becomes smaller, there may be insufficient space for electrolyte and dye penetration, so the $TiO_2$–dye–electrolyte interface is unable to obtain a good electrical contact with each other inside the $TiO_2$ thin film, resulting in lowering the light-to-electricity conversion efficiency. "In fact, the average $TiO_2$ particle size of the dispersion was 380 nm for the sample which has 15 min dispersion time with 0.6–0.8 mm zircon beads. Whereas it was 270 nm for the one of 120 min dispersion time with 0.3 mm zirconia beads. Please note that the particle size tends to be larger compared to actual $TiO_2$ particle size on film. This is probably because the particle size characterization machine measures the $TiO_2$ particle size in a liquid when $TiO_2$ tends to form aggregation more in the liquid, than on the film." It has been reported that when the size of pores in the $TiO_2$ film is too small, the performance of dye-sensitized solar cells deteriorates due to slowed electrolyte diffusion in the film [22]. Nakade et al. [23] also reported that as the $TiO_2$ particles become larger, the electron diffusion coefficient increases and electron recombination lifetime decreases, respectively, resulting in an enhancement of the solar cell performance. It should be noted here that similar phenomena were observed when we used polyvinyl butyral, cellulose acetate butylate, and PEG as resin.

We cannot clearly elucidate why the ethyl cellulose and terpineol combination exhibited the best performance. However, one possible explanation is that the molecular weight of currently used ethyl cellulose enabled us to form a proper pore size among individual $TiO_2$ particles, and a suitable size of spaces within the $TiO_2$ aggregation. Therefore, the electrolyte and dye penetration was optimized inside the film, leading to good electrical contact.

Hereafter, we will refer to this ethyl cellulose and terpineol combination of $TiO_2$ dispersion as the ECT–$TiO_2$ system, whereas water-based PEG $TiO_2$ dispersion as the PEG–$TiO_2$ system. We proceed to compare the performance of organic solvent based $TiO_2$ dispersions with water-based $TiO_2$ dispersions in order to further elucidate the fundamental $TiO_2$ properties of ECT–$TiO_2$ and PEG–$TiO_2$ systems.

Figure 1 shows AFM observations of the PEG–$TiO_2$ and ECT–$TiO_2$ thin films. Particle size seems much larger than the primary particle size of P25 ($\sim$30 nm) especially in the PEG–$TiO_2$ thin film. Particle surface structure was more distinctive in the ECT–$TiO_2$ thin film. In fact, the surface area of the ECT–$TiO_2$ thin film (93.4256 $m^2/g$) was 1.77 times larger than that of the PEG–$TiO_2$ thin film (52.6626 $m^2/g$) measured by BET analysis.

TG–DTA curves for the PEG–$TiO_2$ dispersion and the ECT–$TiO_2$ dispersion are shown in Fig. 2. Regarding the

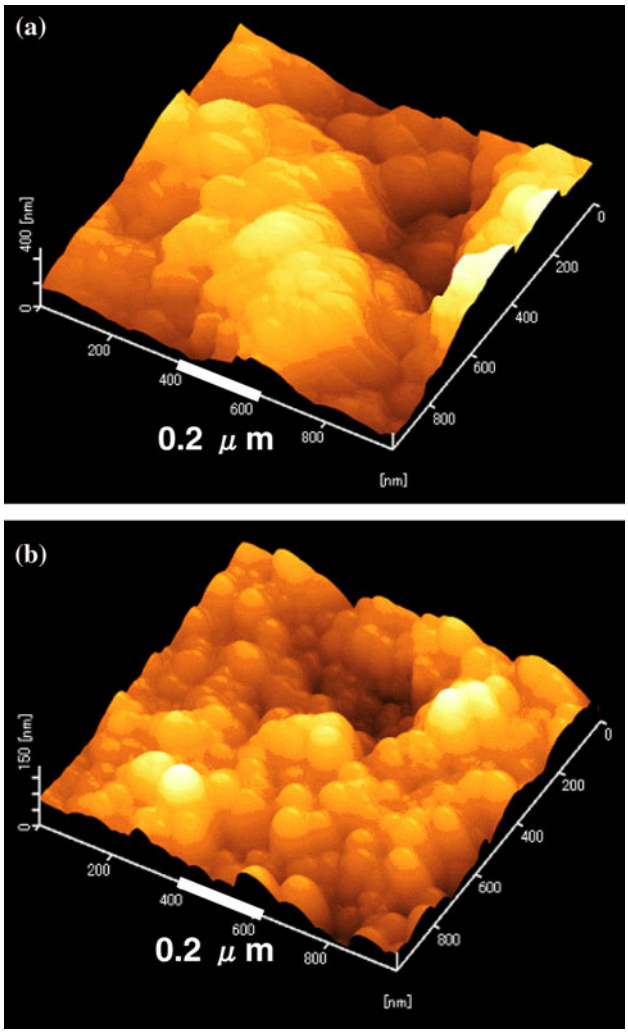


**Fig. 1** AFM observation of the $TiO_2$ thin films. **a** PEG–$TiO_2$ thin film, **b** ECT–$TiO_2$ thin film

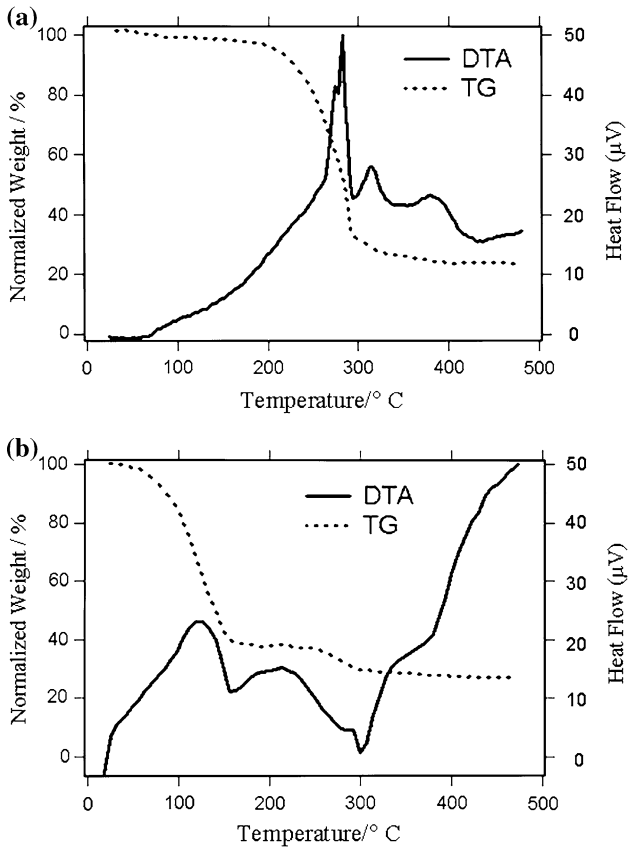


**Fig. 2** TG and DTA curves of $TiO_2$ paste. **a** PEG–$TiO_2$ system, **b** ECT–$TiO_2$ system

PEG–$TiO_2$ dispersion, one can observe a large exothermic peak at 280 °C, which can be attributed to polyethylene glycol decomposition. A small peak can also be observed at 320 °C, which can be attributed to decomposition of the polyoxyethylene (20) sorbitan monolaurate. Regarding the ECT–$TiO_2$ dispersion, an endothermic peak can be seen at 175 °C, which is considered to be due to evaporation of terpineol, since it coincides with the boiling temperature of terpineol. Precisely, the currently used industrial terpineol contains terpineol and limonene. In fact, this small peak coincides with the boiling temperature of limonene more than that of terpineol. The broad peak observable at 295 °C can be explained by decomposition of the ethyl cellulose.

Because the surface area of the ECT–$TiO_2$ thin film is larger than that of the PEG–$TiO_2$ thin film as detected by BET analysis, the ECT–$TiO_2$ thin film therefore possesses more available sites for photoelectrochemically active points since $TiO_2$ film surface area is a critical factor for dye-sensitized solar cells. We suggest this is the reason for showing better performance of ECT–$TiO_2$ system than that of PEG–$TiO_2$ system.

It is also inferred that because the decomposition of resin and solvent peaks are broad in the ECT–$TiO_2$ system, and the boiling temperature of terpineol is much higher than that of water, the $TiO_2$ paste for this system burned out slower from the substrate so that $TiO_2$ film did not crack as much as water-based case, which is often the case when a $TiO_2$ thin film is heat-treated. These fundamental morphology and film formation differences that occur during the heat treatment process thus result in the difference of the energy conversion efficiency.

## Influence of metal doping

We have chosen an ECT–$TiO_2$ system to investigate the effects of metal doping considering this system exhibited a superior solar cell performance as described above.

The $TiO_2$ powder, used in this study, P25, is composed of anatase-form crystals with a 78 wt% and rutile-form crystals with a 22 wt%, and with particle size of 15–30 nm in diameter. The effect of doping on solar energy conversion efficiency ($\eta$) of dye-sensitized solar cells is heavily dependent on the particular metal used as a dopant. Figure 3 shows the conversion efficiency of dye-sensitized solar cells with various metal-doped $TiO_2$ electrodes. It should be noted here that we have extracted the highest conversion efficiency number irrespective of doping concentration. The doping concentration is thus different among the doped $TiO_2$ electrodes shown in Fig. 3. It can be seen that Nb and Ag doping led to a clear enhancement of $\eta$. In order to clarify the effect of meal doping on energy conversion efficiency, the structure of $TiO_2$ powder and

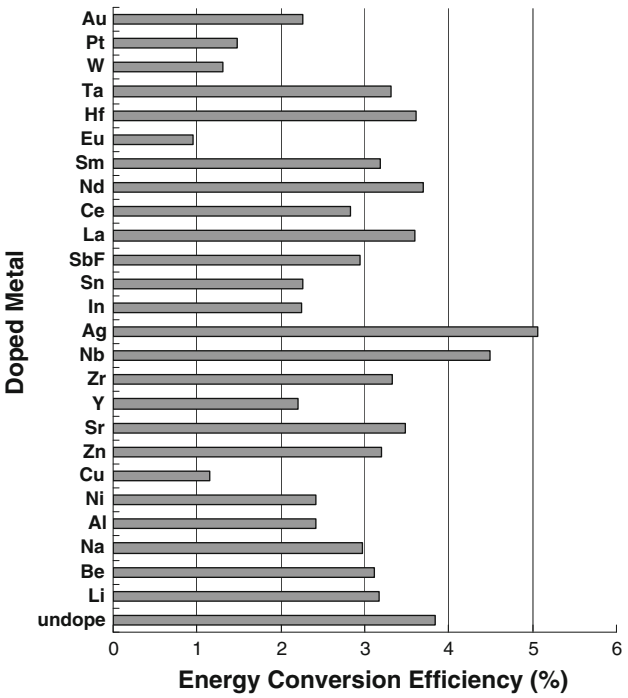


**Fig. 3** Conversion efficiency of DSCs with various metal-doped $TiO_2$ electrodes

**Table 3** Photovoltaic and film characteristic of dye-sensitized solar cells prepared from Nb-doped $TiO_2$ thin film prepared in this study

| Sample | $J_{sc}$, short circuit current (mA/cm$^{-2}$) | $V_{oc}$, open circuit voltage (mV) | FF, fill factor | $\eta$, energy conversion efficiency | BET surface area (m$^2$/g) |
|---|---|---|---|---|---|
| Undoped | 11.01 | 703 | 0.496 | 3.84 | 93.4256 |
| Nb-0.1 | 11.46 | 733 | 0.505 | 4.24 | 56.5474 |
| Nb-1 | 12 | 724 | 0.517 | 4.49 | 53.2952 |
| Nb-5 | 7.05 | 676 | 0.533 | 2.54 | 54.8359 |
| Nb-25 | 4.79 | 583 | 0.563 | 1.57 | 59.7875 |

photovoltaic properties of dye-sensitized solar cells were investigated in detail using Nb and Ag-doped $TiO_2$ electrodes.

Table 3 summarizes the photovoltaic characteristics of $TiO_2$ thin films prepared from niobium doped ECT–$TiO_2$ systems. The best results were obtained for an Nb-1 $TiO_2$ thin film. Energy conversion efficiency decreases as the Nb content increases up to 5:100 = Nb:Ti in molar ratio.

Anatase $TiO_2$ is known to possess interstitial channels in the *c* direction, and so certain transition metals diffuse through these channels into lattices. The diffusing ions have been found to locate preferentially on either the substitutional or interstitial sites. In general, for better $TiO_2$ photoelectrochemical performance, the dopant for $TiO_2$ should satisfy the following three conditions: (1) it should be pentavalent; (2) it should have an ionic radius close to $Ti^{4+}$ (0.64 Å); and (3) it should have an oxide soluble in $TiO_2$ [19]. Niobium seems to be an optimum choice because it is pentavalent ($Nb^{5+}$) and it has similar radius (0.69 Å) to that of $Ti^{4+}$ in $TiO_2$. In addition, Nb can dissolve in $TiO_2$ isotopically, and niobium has been previously reported to be a good dopant for $TiO_2$ [24–26]. In fact, in examining X-ray diffraction patterns of ECT–$TiO_2$, Nb-1 and up to Nb-5 films, none of the Nb-doped films showed peaks corresponding to deposited niobium correlated substance, implying that neither niobium nor niobium oxide is precipitated on the film surface, but is instead doped into $TiO_2$ (data not shown). It has been reported that the $Nb^{5+}$ ions in $TiO_2$ substitute $Ti^{4+}$ isotropically and act as electron donors to reduce $Ti^{4+}$ to $Ti^{3+}$. It also has been elucidated by XPS measurement that the Ti(III) shoulders grow in intensity by Nb doping, especially at very low doping levels [27, 28]. It seems that the increase in the concentration of the donors, such as $Ti^{3+}$, in the $TiO_2$ thin film by Nb doping increases the conductivity, resulting in the higher photocurrents observed in this study. It should be noted here that even though the surface area of the $TiO_2$ thin film decreases with the use of Nb doping (Table 3), Nb-1 $TiO_2$ thin films still showed the best performance.

Table 4 summarizes the photovoltaic characteristics of $TiO_2$ thin films prepared from silver-doped ECT–$TiO_2$ systems. As the amount of Ag dopant increases, solar cell performance improves, especially the photo voltage. The Ag doping can be seen to be most effective for an Ag-1.5 $TiO_2$ film, with $\eta$ reaching 5.07% for this doping, and thereafter decreasing as Ag content increases up to 5:100 = Ag:Ti in molar ratio. Figure 4 shows the XRD patterns of Ag-doped $TiO_2$ powder at various doping concentrations. Diffraction peaks corresponding to anatase-form crystals and rutile-form crystals appear in the XRD pattern of undoped $TiO_2$ powder. In the case of Ag-doped $TiO_2$ powder, diffraction peaks corresponding to both crystal forms again appear. However, a careful observation also takes a notice of the appearance of new diffraction peaks at $2\theta = 44.3°$, 64.5°, and 77.5° indicated by arrows in the figure. These peaks are identified as those of (200), (220), and (311) planes of Ag crystal. The diffraction intensity of these peaks increases with increasing amounts of doping. XPS spectrum of Ag-doped $TiO_2$ powder is

**Table 4** Photovoltaic and film characteristic of dye-sensitized solar cells prepared from Ag-doped $TiO_2$ thin film prepared in this study

| Sample | Particle size (nm) | BET surface area (m$^2$/g) | Amount of adsorbed dye (10–8 mol/cm$^{-2}$) | $J_{sc}$, short circuit current (mA/cm$^{-2}$) | $V_{oc}$, open circuit voltage (mV) | FF, fill factor | $\eta$, energy conversion efficiency |
|---|---|---|---|---|---|---|---|
| Undoped | 21.8 | 93.4 | 5.7 | 6.2 | 717 | 0.5 | 2.21 |
| Ag-0.2 | 20.1 | 54.2 | 6.2 | 7.4 | 745 | 0.51 | 2.78 |
| Ag-0.5 | 18 | 52 | 9.5 | 9.6 | 794 | 0.53 | 4.05 |
| Ag-1.0 | 20.8 | 51.7 | 8.4 | 9.8 | 803 | 0.54 | 4.26 |
| Ag-1.5 | 19.8 | 51.1 | 9.3 | 10.9 | 832 | 0.56 | 5.07 |
| Ag-2.0 | 17.5 | 48.7 | 8.8 | 10 | 831 | 0.58 | 4.81 |
| Ag-5.0 | 21.5 | 43.6 | 5.6 | 1.7 | 607 | 0.72 | 0.75 |

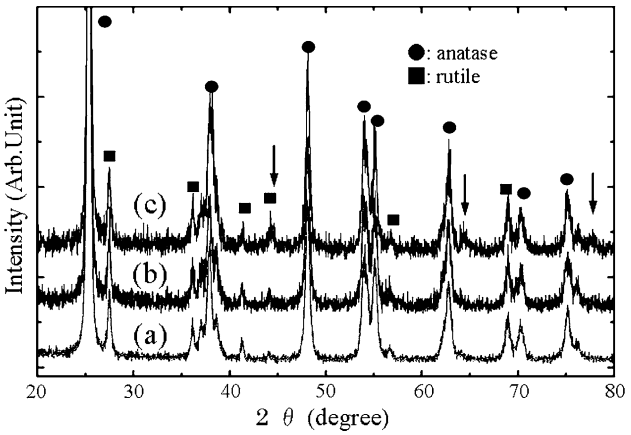


**Fig. 4** XRD patterns of $TiO_2$ electrode (*a*) undoped, (*b*)Ag-1, (*c*)Ag-5

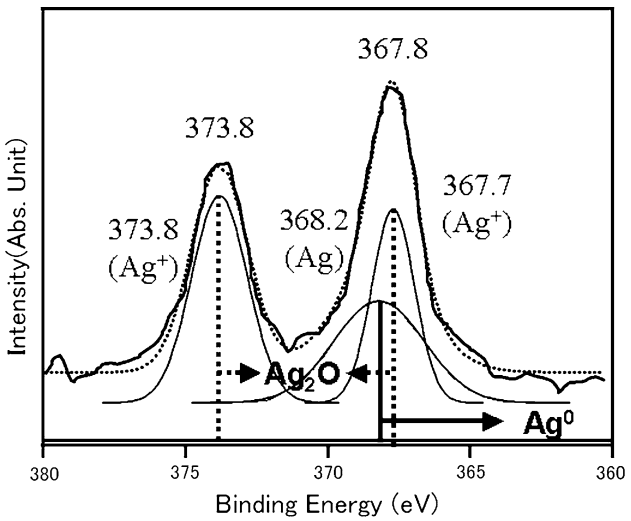


**Fig. 5** XPS-spectra of Ag$3d^{5/2}$ and $3d^{3/2}$ peak of Ag-doped $TiO_2$ powder

shown in Fig. 5. Two bands are observed at 367.8 and 373.8 eV. Former band is in good agreement with $Ag^{+}(3d_{3/2})$. However, latter band is slightly different with $Ag^{+}(3d_{5/2})$. This suggests the coexistence of another element. This band was decomposed to two bands with an intensity ratio of 47:53. The bands with high and low energy are assigned to $Ag^{0}(3d_{5/2})$ and $Ag^{+}(3d_{5/2})$. Therefore, one can say that Ag-doped $TiO_2$ film possess metal Ag and silver oxide which supports the results for X-ray diffraction analysis.

These results indicate that Ag doping does not affect the $TiO_2$ crystalline phase, and doped Ag exists as metal and silver oxide on the surface of $TiO_2$ particles. It seems that carbon created from the organic binder during calcination gives rise to reduction from $Ag^{+}$ to $Ag^{0}$.

TEM observation indicates that the primary particle size of $TiO_2$ was approximately 22–25 nm in diameter (Fig. 6). There is no difference in particle size between the undoped $TiO_2$ and any of the Ag-doped $TiO_2$. This indicates that Ag doping has no significant effect on the $TiO_2$ particle size.

The particle size and surface area of Ag-doped $TiO_2$ particles, along with the amount of adsorbed dye against $TiO_2$ particles, are summarized in Table 4. Specific surface area decreases as the added amount of dopant increases.

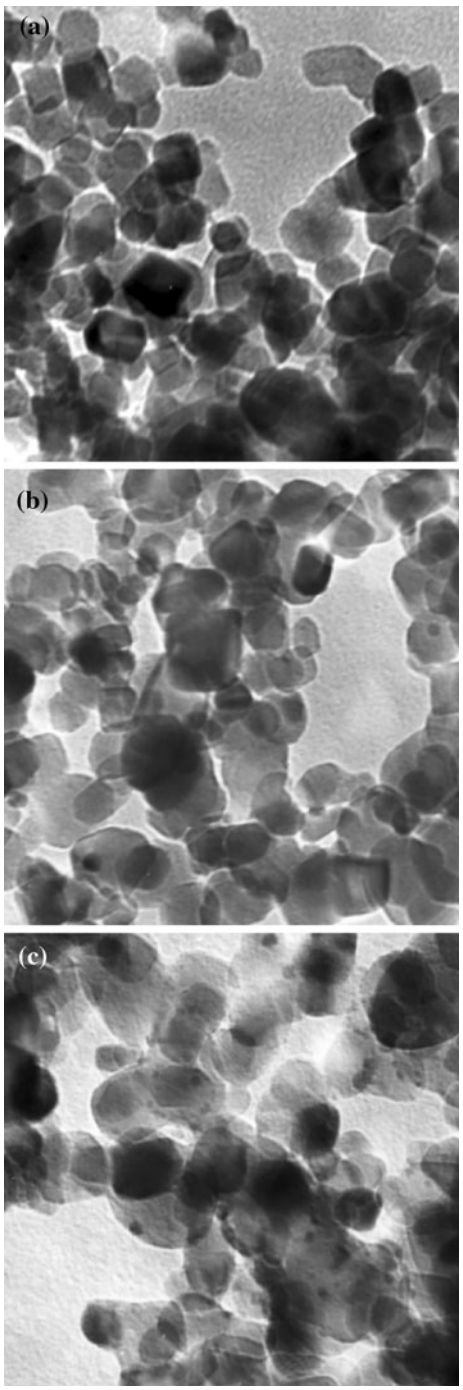


**Fig. 6** TEM Image of $TiO_2$ electrode. **a** undoped $TiO_2$, **b** Ag-1.5, **c** Ag-5

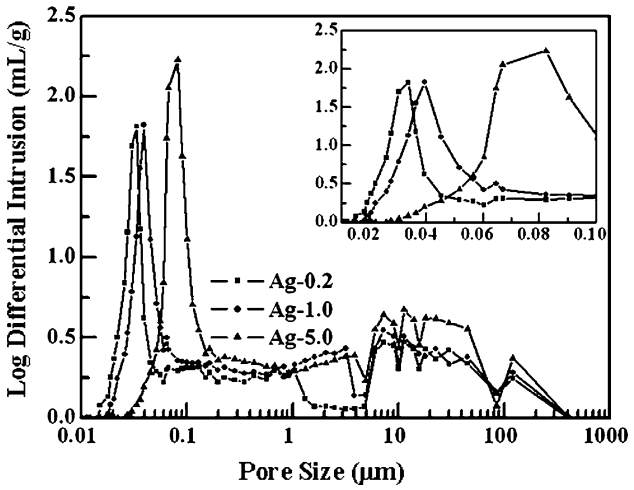


**Fig. 7** Pore size distribution of Ag-doped $TiO_2$ electrodes with various concentrations. *Inset* indicates enlarged distribution curves in the range from 0.01 to 0.10 μm

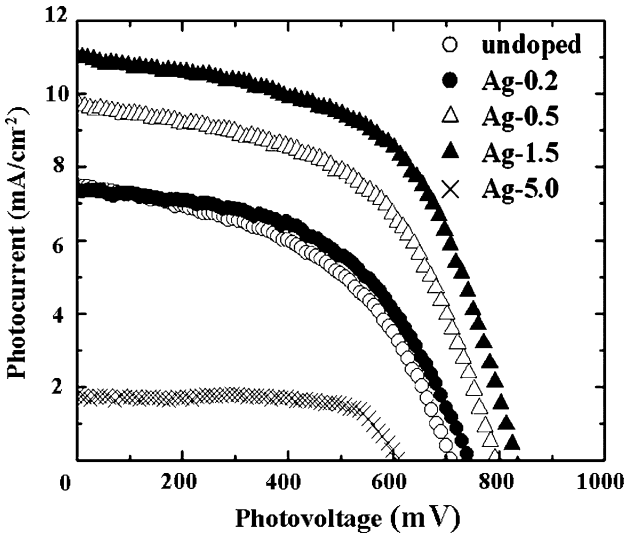


**Fig. 8** *I–V* curves of DSCs using undoped and Ag-doped $TiO_2$ electrodes

On the other hand, the amount of adsorbed dye molecules per unit area increases up to 2.0% doping, and thereafter decreases with further increases in doping.

Figure 7 shows the distribution of pore size of Ag-doped $TiO_2$ particles. There are two peaks in the pore size distribution: a sharp peak with a narrow size, and a broad peak with wide size. The latter appears in the range from 5 to 80 μm independently of the doping concentration. These are suggested to be corresponding to voids between $TiO_2$ agglomerates. On the other hand, the former is corresponding to voids between nanocrystalline $TiO_2$ particles. The pore sizes are 0.0336, 0.0394, and 0.0824 μm in Ag-0.2, Ag-1.0, and Ag-5.0 $TiO_2$ agglomerates, respectively. Ko et al. [29] have reported that surface polarity modified by metal ions could change the primary particle size and dispersibility. It is thus also proposed that Ag doping has an influence on the dispersibility of $TiO_2$ particles. The more the dopant concentration increases, the wider the pore size in the agglomerate. However, the amount of adsorbed dye molecules per unit area increases with dopant concentration in the range from 0.2 to 2.0% in spite of decreases in the specific surface area across this range. This result seems to suggest that the adsorption strength of dye molecules on Ag metal is stronger than that on $TiO_2$. However, the reason for the stronger dye adsorption on Ag remains unknown and needs to be studied. Excess doping, on the other hand, gives rise to an aggregation of $TiO_2$ particles, resulting in a smaller surface area and lower adsorption.

Figure 8 shows photovoltaic current–voltage characteristics of the present $TiO_2$ based dye-sensitized solar cells. It is found that Ag doping is effective at enhancing both photocurrent and photovoltage. The photovoltaic parameters of undoped and Ag-doped $TiO_2$ electrodes are also summarized in Table 4. The current–voltage curve can be described using the following set of parameters: the short circuit current ($I_{sc}$, mA $cm^{-2}$), the open circuit voltage ($V_{oc}$, mV), the efficiency percentage ($\eta$), and the fill factor percentage (FF). $I_{sc}$ is the current that is recorded when the voltage is zero, and $V_{oc}$ is the potential when the current is zero. The efficiency is given by the ratio of the electrical power that is delivered by the cell to the power of the light that is illuminating the cell. The fill factor, FF, is defined as

$$\mathrm{FF} = \frac{(I \times V)_{\max}}{I_{sc} \times V_{oc}} \times 100$$

the energy conversion efficiency, $\eta$, is defined as

$$\eta = \frac{(I \times V)_{\max}}{P_{\text{light}}} = \frac{\mathrm{FF} \times I_{sc} \times V_{oc}}{P_{\text{light}}}$$

where $P_{\text{light}}$ is the incident light intensity.

It is clear that the Ag-1.5 $TiO_2$ electrode shows the best cell performance, in which $I_{sc}$, $V_{oc}$, FF, and energy conversion efficiency are 10.9 mA/$cm^2$, 832 mV, 0.56, and 5.07%, respectively. It should be noted that the concentration of Ag in the Ag-1.5 $TiO_2$ electrode was determined to be 1.06% with more accurate measurement using XPS. From our experimental results, the enhanced solar cell performance of the Ag-1.5 $TiO_2$ electrode is attributed to appropriate pore size and dye adsorption in the $TiO_2$ agglomerate.

$TiO_2$ electrodes with dispersed silver nanoparticles and sensitized dye have been reported in previous research [30–32]. There are several effects that can be related to the change of the photocurrent and photovoltage of the cell between the semiconductor, dye, and the redox electrolyte.

(1) Surface metal particles and the metal particle-induced surface states can electrocatalytically promote the

transportation of UV light-generated holes from the valence band to the electrolyte solution. (2) A strong electromagnetic field is induced by the Ag plasmon, which either enhances the optical absorption of the dye or the surface states of the $TiO_2$ electrodes. (3) Internal photoemission from the Ag particle increases the photocurrent. On the other hand, (4) Schottky barriers at the $TiO_2$/metal interfaces in the interior reduce the mobility of the electrons and holes. (5) The surface metal particles and the metal particle-induced surface states act as recombination centers of light generated electron/hole pairs. (6) The fluctuation of the conduction band edge caused by the surface metal particles retards the transfer of the conduction band electrons from the surface to the interior. Effects (1)–(3) increase the photocurrent, while effects (4)–(6) decrease the photocurrent. In these previous researches, the study by Wen et al. [32] describes how the photoresponse in a longer wavelength in the range of 420–800 nm increases, whereas this response is found to decrease in the studies of Zhao et al study [30, 31]. Investigations of the photoresponse against wavelength of the current Ag-doped ECT–$TiO_2$ system remains an area for future study, but in any case, it seems that the influence of factors (1)–(3) above were stronger in the present study.

### Comparison with general $TiO_2$ paste for dye-sensitized solar cell

It should be noted here that T/SP $TiO_2$ paste (Solaronix SA, Switzerland) made by the hydrothermal method resulted in a conversion efficiency of about 5.5% in our experiment although our best result was about 5%. However, our dispersion technique can be easily transferred to mass production level "bead mill" machine dispersion procedure. This means that we can manufacture a $TiO_2$ liquid dispersion with almost identical performance to that of T/SP at a substantially lower cost. With hydrothermal method in an industrial level, usually only 50–150 kg of titania paste can be manufactured in 1 day and also high temperature is necessary for autoclave. On the other hand, our method can produce over 5–6 tons or ever more at much shorter time. In addition, we do not need high temperature. In a recent research, we have achieved even higher light-to-electricity energy conversion efficiency than present study by using $TiO_2$ with higher anatase crystallinity instead of P25 as a raw material, and also with another dispersion technique, which will be discussed in a forth coming paper.

## Conclusions

We have prepared a $TiO_2$ liquid dispersion of P25 using a general industrial dispersion technique for the $TiO_2$ electrode of a dye-sensitized solar cell. Organic solvent based $TiO_2$ dispersions enabled the formation of more uniform $TiO_2$ thin films in comparison with water-based $TiO_2$ dispersions. The best combination was found to be that using ethyl cellulose as the resin and the terpineol as the solvent. It was also found that using two kinds of resin of different molecular weights, gave rise to better efficiency. To obtain high solar efficiency, hard dispersion condition to breakdown the $TiO_2$ nanoparticle into a small size was not necessary. Because as particle size decreases, dye–electrolyte diffusion is suppressed in the $TiO_2$ thin film, which will lower the solar cell performance. The best metal dopant from the perspective of enhancing the light to electricity conversion efficiency was found to be Ag. This Ag metal doping had an influence on pore size and dispersibility of $TiO_2$ agglomerates, and on the amount of adsorbed dye molecule on the $TiO_2$ electrode, which are proposed as the reasons for the observed enhanced cell performance. Ag-doped $TiO_2$ film possesses metal Ag and silver oxide which supports the results for X-ray diffraction analysis.

**Acknowledgements** This study has been carried out through Collaboration of Regional Entities for the Advancement of Technological Excellence (abbr. CREATE) organized by HYOGO Prefecture and funded by Japan Science and Technology Agency (abbr. JST) for development of common ground of nano-particle composite.

## References

1. O'Regan B, Grätzel M (1991) Nature 353:737
2. Bach U, Lupo D, Comte P, Moser JE, Weissörtel F, Salbeck J, Spreitzer H, Grätzel M (1998) Nature 395:583
3. Nazeeruddin M, Angelis F, Fantacci S, Selloni A, Viscardi G, Liska IS, Takeru B, Grätzel M (2005) J Am Chem Soc 127:16835
4. Xia J, Li F, Yang H, Li X, Huang C (2005) J Mater Sci 42:6412. doi:10.1007/s10853-006-1184-3
5. Hirata N, Lagref JJ, Palomares EJ, Durrant JR, Nazeeruddin MK, Gratzel M, Censo DD (2004) Chem Eur J 10:595
6. Bignozzi CA, Argazzi R, Indelli MT, Scandora F (1994) Sol Energy Mater Sol Cells 32:229
7. Argazzi R, Bignozzi CA, Heimer TA, Castellano FN, Meyer G (1994) Inorg Chem 33:5741
8. Koumura N, Wang ZS, Miyashita M, Uemura Y, Sekiguchi H, Cui Y, Mori A, Mori S, Hara K (2009) J Mater Chem 27:4829
9. Usami A (1997) Chem Phys Lett 277:105
10. Ferber J, Luther J (1998) Sol Energy Mater Sol Cells 54:265
11. Huang SY, Schlichthörl G, Nozik AJ, Grätzel M, Frank AJ (1997) J Phys Chem B 101:2576
12. Nattestad A, Mozer AJ, Fischer MR, Cheng YB, Mishra A, Bauerle P, Bach U (2010) Nat Mater 9:31
13. Schlichthörl G, Huang SY, Sprague J, Frank AJ (1997) J Phys Chem B 101:8141
14. Snaith HJ (2010) Adv Funct Mater 20:13
15. Kavan L, Grätzel M, Rathousky J, Zukal A (1996) J Electrochem Soc 143:394
16. Papageorgiou N, Barbe C, Grätzel M (1998) J Phys Chem B 102:4156
17. Lin B, Aydil ES (2009) J Am Chem Soc 131:3985

18. Frank JA (1997) AIP conference proceedings: future generation photovoltaic technologies: proceedings of the first NREL conference. NICH Report No. 24469:145
19. Finklea HO (1998) Semiconductor electrodes. Elsevier, Amsterdam
20. Zhao G, Kozuka H, Lin H, Yoko T (1996) Thin Solid Films 339:123
21. Zhao G, Kozuka H, Lin H, Yoko T (1996) Thin Solid Films 340:125
22. Barbe CJ, Arendse F, Comte P, Jirousek M, Lezmann F, Shklover V, Grätzel M (1997) J Am Ceram Soc 80:3157
23. Nakade S, Saito Y, Kubo W, Kitamura T, Wada Y, Yanagida S (2003) J Phys Chem B 107:8607
24. Salvador P (1980) Sol Energy Mater 2:413
25. Kutty TN, Avudaithai M (1990) Int J Hydrogen Energy 15:621
26. Kikkawa J, O'Regan B, Anderson MA (1991) J Electroanal Chem 309:91
27. Goodenough JB (1971) Prog Solid State Chem 5:145
28. Morris D, Dou Y, Rebane J, Mitchell CJ, Egdell RG (2000) Phys Rev B 61:13445
29. Ko KH, Lee YC, Jung YJ (2005) J Colloid Interface Sci 283:482
30. Zhao G, Kozuka H, Yoko T (1996) Thin Solid Films 277:147
31. Zhao G, Kozuka H, Yoko T (1996) Sol Energy Mater Sol Cells 277:147
32. Wen C, Ishikawa K, Kishima M, Yamada K (2000) Sol Energy Mater Sol Cells 61:339